ISSN 1330-3651 (Print), ISSN 1848-6339 (Online)
https://doi.org/10.17559/TV-20240719001862
Original scientific paper

A Novel Plane-Based Probe Tip Calibration Method for Stereo Measurement and Navigation

Mingbo LIU, Tieyuan SUN, Ye HAN, Jianshuang LIU, Xiaolong YOU, Lubin LIU*

Abstract: This paper introduces a novel approach for calibrating the probe tip position by confining it on an unknown plane. A stereo-based camera system is utilized to track the six degrees of freedom (6DoF) of a rigid object equipped with markers. With the calibrated probe tip position, the stereo system can ascertain the location of the probe tip through a rigid transformation, even when the probe tip is visually obscured from view. This functionality is of vital importance in industrial measurement and surgical navigation applications, where the probe tips are frequently not visible to cameras. Existing calibration methods commonly involve confining the probe tip within a conical hole or on a spherical surface. In contrast, our proposed method merely requires a small planar surface that is readily accessible in production environments and cost-efficient to implement. Additionally, this approach exhibits significantly reduced susceptibility to shock and vibration due to the inherent invariance of planes along their surfaces. Experimental results suggest that our method attains an accuracy of 0.02 mm (RMS). This progress has significant implications for improving spatial positioning accuracy in surgical robots and navigation systems, thereby providing a theoretical basis for spatial registration before surgical procedures.

Keywords: plane-based; spatial positioning; surgical navigation; tip position

1 INTRODUCTION

A stereo-based camera system uses two cameras to capture the scene of view and calculate position by disparity [1]. The stereo-based measurement has been extensively applied to industrial measurement [2-5], surgical navigation [6-8], auto pilot [9], and AVG (Automated Guided Vehicle) [10] in the last decade. There are two main methods to perform measurement, by contactless scanning [5] or by contacted probing [11, 12]. The scanning method is widely used [5] as it can directly acquire 3D point cloud without contacting with the target. If a scanning device does not actively project pattern to the target, the disparity is computed by matching object features at pixel level. Thus, the accuracy is limited to pixel level. If a scanning device actively projects pattern to the target, the accuracy can be ten times higher (0.1 pixel) by using subpixel edge locating method [13]. When the target is invisible to the scanning device, for example, bones inside a body, the scanning device is not able to acquire data of the target. This is so called hidden measurement. A scanning device cannot scan a deep hole either, because a deep hole is impossible to be visible to two cameras simultaneously.

The probing method on the other hand, like the traditional probing CMM system [11], uses a precise ball to contact with the target to acquire points as shown in Fig. 1.

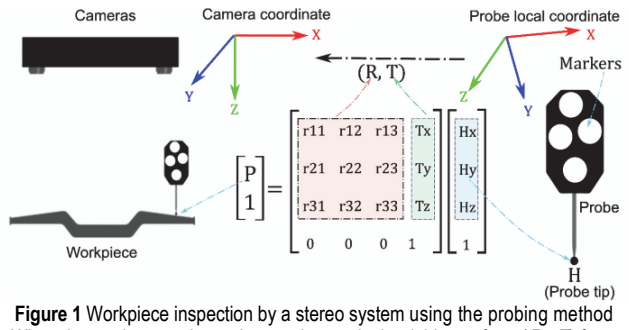

Figure 1 Workpiece inspection by a stereo system using the probing method When the markers on the probe are detected, the rigid transform (R, T) from the probe local coordinate to the camera coordinate is computed. If the position (H) of the probe tip under the probe local coordinate is known, H can be transformed to the camera coordinate by (R, T) so that the position of the probe tip under the camera coordinate is obtained.

Markers are attached to a rigid G so that the cameras can detect the 6DoF of G. The probe local coordinate M can be defined by markers arbitrarily. A ball is mounted to G as the probe tip. If the position H of the probe tip under M is known, the stereo system can compute the positions $\{Pi\}$ of ball centers under the camera coordinate W by applying the rigid transform (R, T) to H, where (R, T) is the rigid transform from M to W and is calculated by the 6DoF of G. Afterward, the measurement can be done with $\{Pi\}$ exactly in the same way as the traditional CMM system does. For example, to fit a plane, a circle etc. by $\{Pi\}$.

If the shape of a marker is circle, the camera can detect the circle center with accuracy at 0.01 pixel level while the depth of view > 3000 mm, due to the symmetry of circle. Meanwhile, as the camera can acquire the position of a ball without the ball being visible to the camera, the probing method can perform hidden measurement for invisible targets and deep holes. The shape of a probe tip can be a sharp needle, where the needle tip is considered as a ball with nearly zero radius. This assumption makes it possible to apply the probing method to surgical navigation where sensing the position of surgical tool needle tip is the main priority, see Fig. 2.

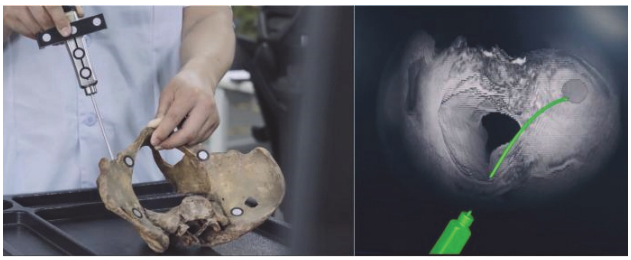

Figure 2 An experimental surgical tool with passive markers. The probe tip is the needle tip

Another important payback of the probing method is that it provides the possibility to perform measurement by a single camera instead of by a stereo system [6, 14]. A single camera is a simpler system to use and is cheaper to equip. A single camera is not capable to acquire depth of a single point in the scene, but it can acquire the 6DoF of a probe with known structure [15]. The tradeoff is lower accuracy,

especially along the depth direction. The purpose of the probe tip calibration is to find out H in the coordinate M, so that the stereo system can calculate the position of the probe tip center H' under W by $H' = RH + T$, where (R, T) is the rigid transform calculated by transforming G from coordinate M to W.

The structure of G can be easily obtained by detecting the centers of markers, but the camera cannot obtain the position of the probe tip H directly. The most straightforward method to calibrate H is to use a conic hole C [12, 16-18] (see Fig. 3).

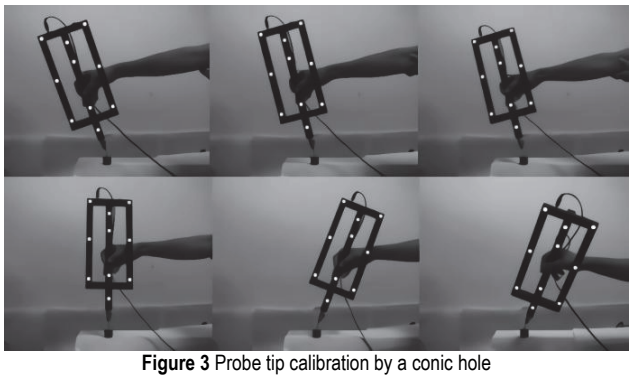

Figure 3 Probe tip calibration by a conic hole
The probe tip is limited to be inside a conic hole, and then rotate the probe to different positions. H is calculated by fitting a sphere [17]

The probe tip is limited to be inside a conic hole, and then rotate the probe to different positions. Liu et al. [17] reported this method with repeatability at about 0.043 mm (standard derivation). If C is a perfect symmetric conic hole and the probe tip is a perfect ball, H' is unchanged when rotating G. Therefore, any marker on G is moving on the surface of a sphere. H is calculated by fitting a sphere.

However, it is hard and expensive to make an accurate conic hole. Besides, it is hard to fix C and the calibration process is very sensitive to shock and vibration. Any movement to the conic hole introduced by external forces, or by hand, will change the position of the fitted sphere center.

The more common calibration method used in the coordinate measurement machine (CMM) field is to use a ball. Limit the probe tip on a sphere while moving G. This method has the same disadvantages as the conic hole method. Moreover, the surface of a ball is very slippery when the ball diameter variation < 5 um. It is quite difficult to hold two such slippery balls contacting each other while performing the calibration. With the fast-growing needs for industrial online measurement and surgical navigation, disadvantages of existing methods limit its application to these fields, where onsite verification and calibration is necessary and shock and vibration is unavoidable. Therefore, this paper proposed a plane-based calibration method, which limits the probe tip on an unknown plane while moving G. A calibration plane is easy to be found in production environment, and the proposed method is far less sensitive to shock and vibration, because a plane is invariant along its surface. There is no accuracy loss compared to existing methods.

In the following sections, the existing conic method is described in detail. Experiments and analyses were carried out to reveal the disadvantages of the conic method. Then based on these experiments and analyses, our plane-based calibration method was proposed. Synthetic data verification was done to verify the proposed method. Finally, real data experiment was done for both the conic method and the proposed method to compare the accuracy and stability.

The conic hole calibration method fixes the probe tip inside a conic hole C as in Fig. 4a.

A typical shape of C is an inversed cone or an inversed sphere. If the probe tip is a sphere S, S is always tangent to C, as C is a continuous and smooth conic surface. Thus, the position of the tip center will stay unchanged when rotating the probe. When rotating the probe, markers on the rigid G are moving on surfaces of different spheres centering at the probe tip center. H then can be calculated by fitting a sphere using positions of markers.

When holding the probe to perform calibration, there are four forces on G, the gravity, the supporting force from C, the force from hand and the friction. It is too difficult for humans to balance these forces to keep the probe tip position unchanged as illustrated in Fig. 4b. As the space limitation of the hole, the space for rotating the probe is restricted to a small angle, as illustrated in Fig. 4c. This limitation decreases the coverage of points for sphere fitting and drops the fitting accuracy.

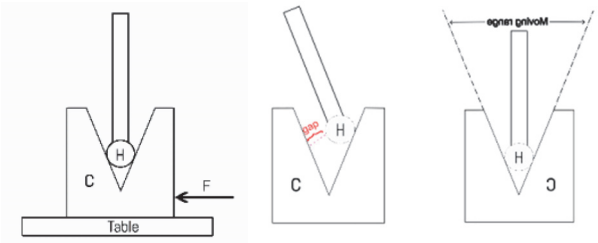

Figure 4 (a) Movement introduced by external forces. The movement is an important error source for sphere fitting. (b) The probe tip may not firmly contact with conic hole because it is hard to balance forces on the probe. (c) The space limitation to move the probe. This limitation decreases the coverage of points for sphere fitting and drops the fitting accuracy

Most importantly, any external force may introduce movement to C. Consequently, the fitted sphere center is sensitive to shock and vibration. External forces such as the force to hold the probe always exist. In this paper, experiments were done to measure the table movement introduced by external forces. Two typical types of tables were tested, a steel table, weight ≈ 200 kg, width = 1.2 m, length = 2.4 m and height = 0.8 m. And a typical office table made of wood, weight ≈ 80 kg, width = 1.2 m, length = 1.2m and height = 0.8 m. The range of force was simulated to cover two major scenarios. One is unavoidable force from holding the probe. And another one is a more intense force introduced by accident, for example, people walk around and hit the table. A dial indicator and a lever arm test indicator are used to monitor the table movement. A force gauge is used to measure the forces. Movements results are shown in Fig. 5.

From the results, the movement introduced by external forces is an important error source for conic calibration method. One should notice that the vertical movement is always < 5 um and far less than the horizontal movement. This is actually the hypothesis the plane-based calibration method initiated from. The vertical movement is very small due to the gravity going vertically.

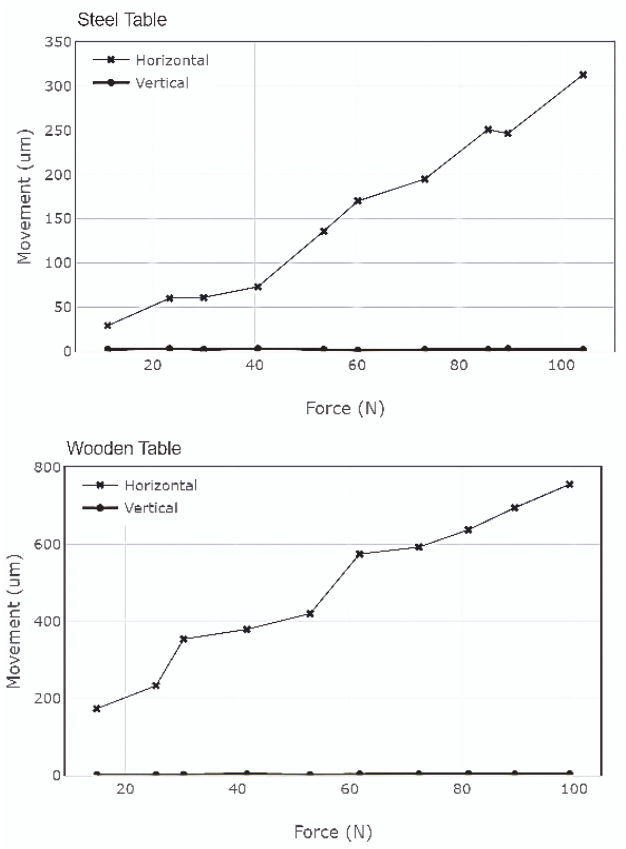

Figure 5 The movement introduced by external forces: (a) Steel table; (b) Wooden table
The movement of the wooden table is significantly higher than the steel table with the same force. The vertical movement is always < 5 um for both steel and wooden table

2 MATERIALS AND METHODS

To solve problems of the conic hole calibration method, the plane-based method is proposed in this paper. The key of the proposed method is to limit the probe tip on an unknown plane instead of a conic hole as illustrated in Fig. 6.

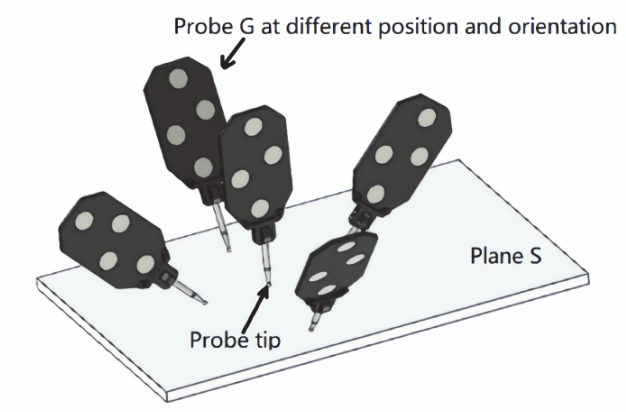

Figure 6 The proposed plane-based calibration method
The probe tip is limited on an unknown plane *S*. Move the probe to different positions and orientations can find out the probe tip center *H*

3 PLANE RESTRICTION

To calibrate the probe tip, move the probe *G* to different positions and orientations while limiting the probe tip contacting with an unknown plane $S(O, N)$, where $O \in R^3$ is any point on S and $N \in R^3$, $\| N \| = 1$ is the normal of S.

The structure of markers on G can be easily obtained by the stereo camera as.

$$G_0 = \{P_{0j} \,|\, P_{0j} \in R^3, j = 1,2...n\}$$

where n is number of markers. A local cartesian coordinate system M can be defined by G_0. The way to define M is not important as long as it is locally defined on G_0. The calibration problem is to find out the position of the tip center $\boldsymbol{H}$ under $\boldsymbol{M}$.

When the probe is moved to an arbitrary position, use the stereo camera to capture the structure of markers under the stereo camera coordinate $\boldsymbol{W}$ as i-th frame:

$$G_i = \{ P_{ij} \,|\, P_{ij} \in R^3 \ \}$$

Then the rigid transform $(\boldsymbol{R}_i, \boldsymbol{T}_i)$ from G_0 to G_i can be calculated, where $\boldsymbol{R}_i$ is a 3-by-3 rotation matrix, and $\boldsymbol{R_i}$ satisfies:

$$R_i^T = R_i^{-1}$$
$$R_i^T R_i = R_i R_i^T = I$$

where $\boldsymbol{I}$ amid entity matrix, and $\boldsymbol{T}_i$ is translating vector:

$$T_i = \begin{bmatrix} t_{xi} & t_{yi} & t_{zi} \end{bmatrix}$$

Apply the rigid transform to $\boldsymbol{H}$, the probe tip center under the coordinate $\boldsymbol{W}$ is

$$P_i = R_i H + T_i$$

If probe tip is firmly contacted with plane $\boldsymbol{S}$ ($\boldsymbol{O}$,$\boldsymbol{N}$), the centers of probe tip must also be on a plane S' (O' , $\boldsymbol{N}$) that satisfies

$$S' // S$$
$$(O' - O)\, N^T = r$$
$$(P_i - O')\, N^T = 0$$

where r is probe tip radius. So

$$(R_i H + T_i - O')N^T = 0 \qquad (1)$$

If any two point $\boldsymbol{P}$ and $\boldsymbol{Q}$ is on a plane, so that

$$(P - O)\, N^T = 0$$
$$(Q - O)\, N^T = 0$$

We have

$$[(Q - O) + (P - O)]N^T = 0$$
$$[(Q + P)/2 - O]N^T = 0$$

That is to say, the average of $\boldsymbol{P}$ and $\boldsymbol{Q}$ is also on the plane. This can be easily extended to any number of points on plane, namely, the average of $\boldsymbol{P}_i$ is on plane $\boldsymbol{S}'$. $\boldsymbol{O}'$ can be replaced by the averaged point as there is no restriction on where $\boldsymbol{O}'$ is, as long as it is on $\boldsymbol{S}'$:

$$\begin{aligned} O' &= P_i \\ &= \frac{\sum_{1}^{n} P_i}{n} \\ &= \frac{\sum_{1}^{n} \left(R_i H + T_i\right)}{n} \\ &= \frac{\sum_{1}^{n} \left(R_i H\right)}{n} + \frac{\sum_{1}^{n} T_i}{n} \\ &= R_i H + T_i \end{aligned}$$

Replace O' in (1)

$$\begin{aligned} &[R_i H + T_i - (R_i H + T_i)] N^T = 0 \\ &\left[\left(R_i - R_i\right) H + T_i - T\right] N^T = 0 \end{aligned} \tag{2}$$

$\boldsymbol{R}_i$ and $\boldsymbol{T}_i$ are known parameters, redefine them to

$$\begin{aligned} R_i &= R_i - R_i \\ T_i &= T_i - H_i \end{aligned}$$

(2) can be re-written to

$$(R_i H + T_i) N^T = 0 \tag{3}$$

In the following sections, $\boldsymbol{R}_i$ and $\boldsymbol{T}_i$ refers to the redefined version unless it is stated.

(3) is plane restriction equation for plane-based calibration method. It should be noticed that redefined $\boldsymbol{R}_i$ is no longer a rotation matrix but a general 3-by-3 matrix. Generally

$$\begin{aligned} R_i^T &\neq R_i^{-1} \\ R_i^T R_i &\neq R_i R_i^T \neq I \end{aligned}$$

Non-Linear Least Square

(3) is non-linear problem [19, 20] and cannot be solved analytically. The Non-linear least square method is used to solve the problem.

The distance from $\boldsymbol{P}_i$ to $\boldsymbol{S}'(\boldsymbol{O}', \boldsymbol{N})$ is

$$e_i = \left(R_i H + T_i\right) N^T \tag{4}$$

The least square problem is to find the best ($\boldsymbol{H}$,$\boldsymbol{N}$) so that

$$\arg\min \sum \left\| F_{i(H,N)} \right\|^2 \tag{5}$$

where

$$F_{i(H,N)} = e_i = \left(R_i H + T_i\right) N^T \tag{6}$$

As (5) is a complicated non-linear problem, iterative numeric minimization algorithm like Gauss-Newton algorithm (GNA) [19], Gradient-Decent algorithm (GDA) [19] can be used to find the best solution. Levenberg-Marquardt algorithm (LMA) [21] is used in this paper for the problem (5) as LMA algorithm is more robust to local minimum issue.

3.1 Initial Guess

Although LMA is more robust to local minimum issue, if the initial value starts in a wrong local minimum zone, LMA may not be able to get out of that zone. So, a better initial value yields higher possibility to the true solution, and faster convergence.

3.1.1 Initial guess - *N*

Place the probe at 3 different non-collinear positions and try to keep the probe at similar orientation as illustrated in Fig. 7.

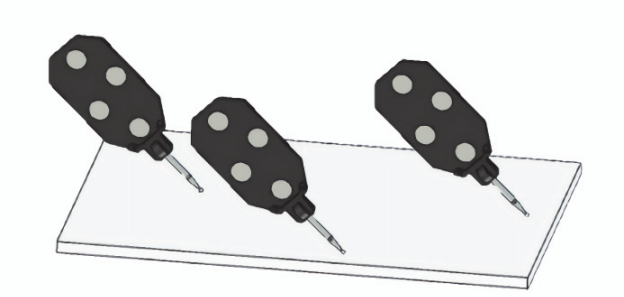

Figure 7 Place the probe at 3 different non-collinear position and try to keep the probe at similar orientation

The initial value of *N* can be calculated.

Pick any marker of *G*, marker 1 for example, the position of marker 1 at these positions under *W* is Q_1, Q_2, Q_3 respectively. Q_1, Q_2, Q_3 define a plane S'' (O'', N'') which is approximately parallel to S (O, N). The normal N'' of S'' can be used as the initial value of the normal of plane S.

$$N'' = \left(Q_2 - Q_1\right) \times \left(Q_3 - Q_1\right) \tag{7}$$

It is not difficult to keep the probe at similar orientation at different position. Besides, the stereo camera can detect the orientation on the fly, so it is possible to guide user to adjust orientation.

3.1.2 Initial guess - *H*

From (3)

$$R_i H N^T + T_i N^T = 0$$

Because $\boldsymbol{H}$ and $\boldsymbol{N}$ is vector $\in R^3$, and $\boldsymbol{R}$ is 3- by-3 matrix, it can be proven (later in this section)

$$R_i H N^T = (R_i^T N) H^T \tag{8}$$

So

$$(R_i^T N) H^T + T_i N^T = 0$$

$\boldsymbol{R}_i$ and $\boldsymbol{T}_i$ are measured by the stereo cameras, and the initial guess of $\boldsymbol{N}$ is known by (7), this is a linear problem with one variable $\boldsymbol{H}$

$$\begin{bmatrix} a_i & b_i & c_i \end{bmatrix} \begin{bmatrix} h_x \\ h_y \\ h_z \end{bmatrix} + \begin{bmatrix} t_{xi} & t_{yi} & t_{zi} \end{bmatrix} \begin{bmatrix} n_x \\ n_y \\ n_z \end{bmatrix} = 0$$

$$\begin{aligned}
R_i H N^T &= \begin{bmatrix} r_{11} & r_{12} & r_{13} \\ r_{21} & r_{22} & r_{23} \\ r_{31} & r_{32} & r_{33} \end{bmatrix} \begin{bmatrix} h_x & h_y & h_z \end{bmatrix} \begin{bmatrix} n_x \\ n_y \\ n_z \end{bmatrix} \\
&= \begin{bmatrix} h_x r_{11} + h_y r_{21} + h_z r_{31} \\ h_x r_{12} + h_y r_{22} + h_z r_{32} \\ h_x r_{13} + h_y r_{23} + h_z r_{33} \end{bmatrix}^T \begin{bmatrix} n_x \\ n_y \\ n_z \end{bmatrix} \\
&= n_x(h_x r11 + h_y r21 + h_z r31) + n_y(h_x r12 + h_y r22 + h_z r32) + n_z(h_x r13 + h_y r23 + h_z r33) \\
&= h_x(n_x r11 + n_y r12 + n_z r13) + h_y(n_x r21 + n_y r22 + n_z r23) + h_z(n_x r31 + n_y r32 + n_z r33) \\
&= \begin{bmatrix} n_x r_{11} + n_y r_{12} + n_z r_{13} \\ n_x r_{21} + n_y r_{22} + n_z r_{23} \\ n_x r_{31} + n_y r_{32} + n_z r_{33} \end{bmatrix}^T \begin{bmatrix} h_x \\ h_y \\ h_z \end{bmatrix} \\
&= \begin{bmatrix} r_{11} & r_{12} & r_{13} \\ r_{21} & r_{22} & r_{23} \\ r_{31} & r_{32} & r_{33} \end{bmatrix}^T \begin{bmatrix} n_x & n_y & n_z \end{bmatrix} \begin{bmatrix} h_x \\ h_y \\ h_z \end{bmatrix} \\
&= (R_i^T N) H^T
\end{aligned}$$

3.2 Jacobian Matrix

To use LMA as iterative optimization, Jacobian matrix [23] is strongly recommended to be provided. With Jacobian matrix as the least square derivations, the iterative optimization converges much faster than other derivations method like numeric derivation method [24] and automatic derivation method [23].

When (5) comes to minimum

$$\begin{aligned}
g_{(H,N)} &= \nabla \sum \left\| F_{(H,N)} \right\|^2 \\
&= \sum \nabla \left\| F_{(H,N)} \right\|^2 \\
&= \frac{1}{2} \sum (F_{(H,N)} \nabla F_{(H,N)}) \\
&= 0
\end{aligned}$$

$$a_i h_x + b_i h_y + c_i h_z + d_i = 0 \tag{9}$$

where

$$\begin{bmatrix} a_i & b_i & c_i \end{bmatrix} = R_i^T N$$

$$d_i = T_i N^T \tag{9}$$

Is a plane equation where the plane cross origin and the normal is H. Thus (9) can be solved by regular least square for plane fitting or by singular value decomposition [22].

Now back to prove equation (8)

$$\begin{aligned}
\frac{\partial F_{(H,N)}}{\partial H} &= \frac{\partial (RHN^T + TN^T)}{\partial H} \\
&= \frac{\partial (RHN^T)}{\partial H} + \frac{\partial (TN^T)}{\partial H} \\
&= \frac{\partial \left[(R^T N)^T H \right]}{\partial H} \\
&= (R^T N)^T
\end{aligned} \tag{10}$$

$$\begin{aligned}
\frac{\partial F_{(H,N)}}{\partial N} &= \frac{\partial \left[RHN^T + TN^T \right]}{\partial N} \\
&= \frac{\partial \left[(RH)^T N \right]}{\partial N} + \frac{\partial \left[T^T N \right]}{\partial N} \\
&= (RH)^T + T^T \\
&= (RH + T)^T
\end{aligned} \tag{11}$$

3.3 Levenberg-Marquardt Iteration

The Ceres-solver library [25] is used to perform Levenberg-Marquardt optimization. To use Ceres-solver, three things are required: (a) initial values as Eq. (7) insection 3.3.1 and Eq. (9) in section 3.3.2, (b) residual Eq. (4) in section 3.2, (c) Jacobian matrix Eq. (10) and Eq. (11) insection 3.4.

There are two variables ($\boldsymbol{H}$,$\boldsymbol{N}$) to solve. However, $\boldsymbol{N}$ only has two degrees of freedom because $\boldsymbol{N}$ is saleable, for example, $\boldsymbol{N}$ = (100, 0, 0) is equivalent to $\boldsymbol{N}$ = (1, 0, 0). The extra freedom makes iteration unstable to converge. The solution is to solve ($\boldsymbol{H}$,$\boldsymbol{N}$) in constrained way, subject to II$\boldsymbol{N}$II = 1. Or define $\boldsymbol{N}$ in sphere coordinate as

$$\begin{aligned} n_x &= \sin(\alpha)\sin(\beta) \\ n_y &= \sin(\alpha)\cos(\beta) \\ n_z &= \cos(\alpha) \end{aligned}$$

Where $\alpha \in [0, \pi]$ and $\beta \in [0, 2\pi)$

Redefine $\boldsymbol{N}$ related Jacobian matrix to

$$\begin{aligned} \frac{\partial F_{(H,\alpha,\beta)}}{\partial \alpha} &= \frac{\partial F_{(H,N)}}{\partial N}\frac{\partial N}{\partial \alpha} \\ &= (RH+T)^T \frac{\partial N}{\partial \alpha} \\ &= \frac{\partial N^T}{\partial \alpha}(RH+T) \\ &= \begin{bmatrix} \frac{\partial \sin(\alpha)\sin(\beta)}{\partial \alpha} \\ \frac{\partial \sin(\alpha)\cos(\beta)}{\partial \alpha} \\ \frac{\partial \cos(\alpha)}{\partial \alpha} \end{bmatrix}(RH+T) \\ &= \begin{bmatrix} \cos(\alpha)\sin(\beta) \\ \cos(\alpha)\cos(\beta) \\ -\sin(\alpha) \end{bmatrix}(RH+T) \end{aligned} \tag{12}$$

$$\begin{aligned} \frac{\partial F_{(H,\alpha,\beta)}}{\partial \beta} &= \begin{bmatrix} \frac{\partial \sin(\alpha)\sin(\beta)}{\partial \beta} \\ \frac{\partial \sin(\alpha)\cos(\beta)}{\partial \alpha} \\ \frac{\partial \cos(\alpha)}{\partial \beta} \end{bmatrix}(RH+T) \\ &= \begin{bmatrix} \sin(\alpha)\cos(\beta) \\ -\sin(\alpha)\sin(\beta) \\ 0 \end{bmatrix}(RH+T) \end{aligned} \tag{13}$$

Both (12) and (13) are scalar value.

4 RESULTS

4.1 Synthetic Data Verification

Synthetic data were generated to verify the proposed method. The data is simulated by:

1. Prepare the probe structure: Manually generate a probe structure G_0, which is composed of 4 points and a probe tip position H_0 in the local coordinate M. The choice of M does not matter. The structure is used for all synthetic tests.

2. Prepare the calibration plane: Fix a plane S_0 (O_0, N_0) in the world coordinate W. The choice of W and S_0 does not matter. For verification convenience, N_0 is set to Z axis.

3. Move the probe: Randomly generate a rigid rotation R_i and a position Q_i on S_0. Then a transform (R_i, $Q_i - R_iH_0$) is calculated to move the probe from probe local coordinate M to be on S_0 in W. The transform is also used to transform the probe structure G_0 to the world coordinate W as G_i.

4. Simulate shock: To simulate table movement, random error was added to Q_i.

5. Repeat step 3 and step 4 to generate n positions.

6. Calibrate: Use G_0 and G_i as input to the plane-based calibration to calculate the probe tip H.

7. Verify: Calculate the difference between H_0 and H as calibration error.

8. Repeat step from 3 to 7 to simulate 1000 test cases.

4 configurations of random error were tested, ranging from 0 to 1.0 mm to simulate the table horizontal movement. Random error within 5 um is added to the plane normal direction to simulate vertical movement. Each configuration includes

1000 test cases. Z axis is perpendicular to plane S_0.

As the result shown in Tab. 1, the table movement in horizontal direction has almost no impact on calibration error, which is consistent with the assumption for the plane calibration method.

Table 1 Synthetic verification for the proposed method
A maximum 1.0 mm error is simulated for the table horizontal random movement. Vertical movement is simulated within 5 um.

Set	Simulated error (um)[1]			Calibration error (um)[2]		
	X	*Y*	*Z*	*X*	*Y*	*Z*
1	0	0	0	0	0	0
2	100	100	5	2	2	4
3	200	200	5	2	2	5
4	1000	1000	5	4	4	10

1 Error is randomly generated within $\pm$ simulated error.
2 By U95. U95 = 2 * standard derivation.

4.2 Real Data Verification

4.2.1 Calibration Repeatability

The plane-based calibration was tested on a steel table in the lab to acquire base line data and on a shaky wooden table to simulate real production environment. The conic method was also tested and used for comparison. Stereo cameras were used to capture (R_i, T_i).

For the steel table in the lab, no shock was simulated. The conic hole calibration was done very carefully on the steel table. Shock was simulated to the wooden table. A dial indicator and a lever arm test indicator were used to monitor the table movement. The maximum movement along horizontal direction was about 0.7 mm and vertical movement < 5 um.

The proposed method was tested directly on the steel table surface as the surface is flat enough. A gauge block was used as the calibration plane on the wooden table. An inversed sphere conic hole was used for the conic method. Each method was calibrated 10 times on each table. The

distribution (repeatability) of calibrated result is shown in Fig. 8.

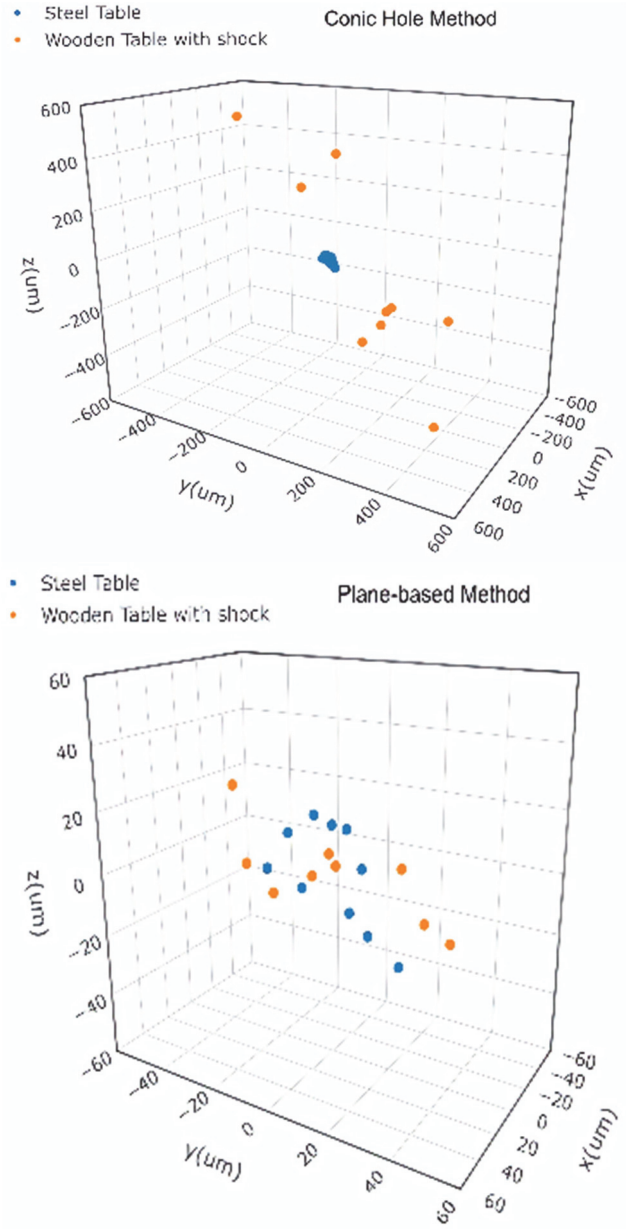

Figure 8 Real calibrated result distribution (repeatability)
No shock was added to the steel table but was added to the wooden table along one direction. The maximum movement was about 0.7 m in horizontal direction, and < 5 um in vertical direction. (a) Conic hole method. Standard derivation = 250 um on the wooden table. (b) Plane-based method. Standard derivation = 15 um on the wooden table

From the test result, the proposed method yielded similar result for both tables. The standard derivation is 15 um. The conic method has similar repeatability on the steel table as the proposed method, but is messed upon the wooden table. The standard derivation reaches 250 um on the wooden table. The maximum derivation is about 500 um, which is closed to the magnitude of movement in the horizontal direction. The proposed method is far less sensitive to shock.

4.2.2 Accuracy Verification

A gauge block was used to verify the absolute accuracy of calibrated result. Related work [17] verified calibration result by measuring length or radius of a workpiece with known size. However, this verification method cannot reveal calibration error in all directions. Assume there is an off- set V (error) between the true probe tip and the calibrated tip. When measure a circle with the calibrated probe tip by n points, and if the probe is held at same orientation, the offset between the measured circle and the true circle is V, but the measured radius is exactly the same as the true value. So simply verify the calibration result by measuring length or radius cannot reveal calibration error in all directions.

In our experiment, a gauge block was used to verify the calibration error as shown in Fig. 9.

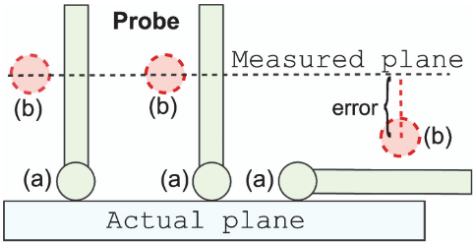

Figure 9 Verify accuracy by measuring the same plane from different directions
The expected distance is zero. (a)The actual probe tip. (b)The calibrated probe tip. When there is an offset (error) between the calibrated tip and the true tip, then the distance will not be zero. The distances fully reflect the calibration error.

The basic idea is to measure the same plane by placing the probe at different orientations. Distance between the same plane certainly should be 0. If the measured distance from all orientations is closed to zero, it indicates the calibration result is consistent in all directions.

Cross test was also performed to measure the same plane by a probe calibrated by the conic hole method and a probe calibrated by the proposed method. The calibration results of two methods are consistent if the distance is zero. Let α denote the angle between the probe rod (where the probe tip is attached to) and the measuring plane on the gauge block. Measure the plane by, for example, $\alpha = 0$, then measure the plane again with $\alpha = 90$. Rotate the gauge block to be parallel to X, Y, Z axis in the stereo coordinate respectively to verify the consistence of the probe tip in X, Y, Z direction. All tests were performed on the steel table in the lab without shock. The results are shown as in Tab. 2.

Table 2 A gauge block was used to verify the probe calibration
Probe A was used to measure a plane on the gauge block, angle = α. Then another probe B was used to measure the same plane, angle = β. The expected distance between two measured planes is 0. Where Z axis runs in the camera depth direction.

Set	Direction 1	Probe 1	α[2]	Probe 2	β[2]	Error (um)[3]
1	Z	Conic	90	Conic	45	3
2	Z	Conic	90	Conic	–45	6
3	Z	Plane	90	Conic	45	5
4	Z	Plane	90	Conic	–45	4
5	Z	Conic	90	Conic	45	10
6	Z	Conic	90	Conic	–45	12
7	Z	Plane	90	Conic	45	8
8	Z	Plane	90	Conic	–45	6
9	X	Conic	90	Conic	60	38
10	X	Conic	90	Conic	–60	34
11	X	Plane	90	Conic	60	24
12	X	Plane	90	Conic	–60	18
13	X	Conic	90	Conic	60	16
14	X	Conic	90	Conic	–60	26
15	X	Plane	90	Conic	60	33
16	X	Plane	90	Conic	–60	38

Standard Derivation = 20 um

1 The axis perpendicular to the measuring plane.

2 Angle (degree) between the probe rod and the measuring plane.

3 Distance (um) between plane measured by probe 1 and probe 2. The expected value = 0.

From test result, the plane-based calibration error achieves micron level (standard derivation) in the *XY* plane. The max error is about 0.04 mm (standard derivation = 0.02 mm) along *Z* axis. And there is no accuracy loss compared to the conic hole method.

5 DISCUSSION

The proposed method uses stereo cameras to capture (R_i, T_i) of a probe to find out the probe tip center H. This method can also be applied to find Tool Center Point (TCP) for a robotic arm, where (R_i, T_i) is captured by the robotic arm instead of stereo cameras. Traditional way to calibrate TCP is to use a sphere or a cone. It is painful to drag the arm and limit the TCP on the surface of a sphere or rotate it around a fixed point in a cone. It is much easier to drag the arm to move along a plane. The proposed method is an alternative option when it is difficult to calibrate TCP in the traditional way. This is also true for articulated measurement arms. A measurement arm needs to be re-calibrated from time to time or use a cone to do frog jumping.

For augmented reality and virtual reality, it is possible to use low-cost stereo cameras or single camera to track probes. With the proposed method, users can make a low-cost probe by his own, for example, a probe based on a pen. And then do probing measurement with mobile phone as the single camera system. With the probe, users can measure objects from small to large (few meters), in both visible and hidden area. Especially in current surgical navigation, the presence of soft tissue coverage makes it difficult to achieve precise spatial registration for certain procedures that require invasive operations. Relying solely on external markers for spatial registration is challenging. By using this technology, virtual imaging can simulate operations within enclosed spaces, such as liver puncture, kidney puncture, and female pelvic floor surgery navigation. Additionally, this method can be extended to other fields, such as the possibility of DIY low-cost VR and AR accessories.

6 CONCLUSION

The calibrated result of the proposed method in production environment is consistent with the result calibrated in the lab. And there is no accuracy loss compared to the conic hole method. More specifically, the calibration error < 0.015 um (U95) in the *XY* plane when there is random shock < 0.7 mm in the horizontal direction. Error along the *Z* axis is about 0.04 mm (U95), and the standard derivation is about 0.02 mm.

The proposed method is insensitive to horizontal movement. Calibration can be done on a regular table in production environment. And the proposed method requires a small area (few cm square wide) of an unknown plane S. A small plane with flatness at micron level is easy to be found in production environment, such as working table, high quality work piece, gauge block, glass, and even mobile screen.

Compared to the conic hole and the sphere method, the proposed method is easy and comfortable for calibration. Simply hold the probe and place the probe tip on a plane, there is no not-firmly contacting concerns nor slippery sphere issue.

Acknowledgments

This work was supported by Chongqing Municipal Bureau of Science and Technology Natural Science Foundation (key projects) (cstc2020jcyj-zdxmX0002), Chongqing Medical Scientific Research Project (2023DBXM001), Chongqing Yuzhong District Science and Technology Bureau Basic research and frontier exploration (20210181) and Medical Research Project of Chongqing Municipal Health Commission (2023WSJK058), and Chongqing Municipal Bureau of Science and Technology Natural Science Foundation (CSTB2022NSCQ-MSX0264).

Figure legends

Figure 1: Workpiece inspection by a stereo system using the probing method. When the markers on the probe are detected, the rigid transform (R, T) from the probe local coordinate to the camera coordinate is computed. If the position ($\boldsymbol{H}$) of the probe tip under the probe local coordinate is known, $\boldsymbol{H}$ can be transformed to the camera coordinate by (R, T) so that the position of the probe tip under the camera coordinate is obtained.

Figure 2: An experimental surgical tool with passive markers. The probe tip is the needle tip.

Figure 3: Probe tip calibration by a conic hole. The probe tip is limited to be inside a conic hole, and then rotate the probe to different positions. $\boldsymbol{H}$ is calculated by fitting a sphere. Cited from [17].

Figure 4: (a) Movement introduced by external forces. The movement is an important error source for sphere fitting. (b) The probe tip may not firmly contact with conic hole because it's hard to balance forces on the probe. (c) The space limitation to move the probe. This limitation decreases the coverage of points for sphere fitting and drops the fitting accuracy.

Figure 5: The movement introduced by external forces. (a) Steel table. (b) Wooden table. The movement of the wooden table is significantly higher than the steel table with the same force. The vertical movement is always < 5 um for both steel and wooden table.

Figure 6: The proposed plane-based calibration method. The probe tip is limited on an unknown plane *S*. Move the probe to different positions and orientations can find out the probe tip center H.

Figure 7: Place the probe at 3 different non-collinear position and try to keep the probe at similar orientation. The initial value of $\boldsymbol{N}$ can be calculated.

Figure 8: Real calibrated result distribution (repeatability). No shock was added to the steel table but was added to the wooden table along one direction. The maximum movement was about 0.7 m in horizontal direction, and < 5 um in vertical direction. (a) Conic hole method. Standard derivation = 250 um on the wooden table. (b) Plane-based method. Standard derivation = 15 um on the wooden table.

Figure 9: Verify accuracy by measuring the same plane from different directions. The expected distance is zero. (a) The actual probe tip. (b) The calibrated probe tip. When there is an offset (error) between the calibrated tip and the true tip, then

the distance will not be zero. The distances fully reflect the calibration error.

7 REFERENCES

[1] Zhang, Z. (1998). Determining the epipolar geometry and its uncertainty: A review. *International Journal of Computer Vision*, *27*(2), 161-195. https://doi.org/10.1023/A:1007941100561

[2] Faugeras, O., Luong, Q. T., & Papadopoulo, T. (2001). The geometry of multiple images: The laws that govern the formation of multiple images of a scene and some of their applications. *MIT Press*. https://doi.org/10.1108/k.2002.06731eae.001

[3] Nister, D. (2004). An efficient solution to the five-point relative pose problem. *IEEE Transactions on Pattern Analysis and Machine Intelligence*, *26*(6), 756-770. https://doi.org/10.1109/TPAMI.2004.17

[4] Scaramuzza, D., Martinelli, A., & Siegwart, R. (2006). A flexible technique for accurate omnidirectional camera calibration and structure from motion. *Proceedings of the IEEE International Conference on Computer Vision Systems*, 45-52. https://doi.org/10.1109/ICVS.2006.3

[5] Sturm, P. & Ramalingam, S. (2004). A generic concept for camera calibration. *Proceedings of the European Conference on Computer Vision*, 1-13. https://doi.org/10.1007/978-3-540-24671-8_1

[6] Triggs, B., McLauchlan, P. F., Hartley, R. I., & Fitzgibbon, A. W. (2000). Bundle adjustment - A modern synthesis. *Vision algorithms: Theory and practice*, 298-372. https://doi.org/10.1007/3-540-44480-7_21

[7] Seitz, S. M. & Dyer, C. R. (1999). Photorealistic scene reconstruction by voxel coloring. *International Journal of Computer Vision*, *35*(2), 151-173. https://doi.org/10.1023/A:1008176507526

[8] Debevec, P. E., Taylor, C. J., & Malik, J. (1996). Modeling and rendering architecture from photographs: A hybrid geometry- and image-based approach. *Proceedings of the 23rd annual conference on Computer Graphics and Interactive Techniques*, 11-20. https://doi.org/10.1145/237170.237191

[9] Pollefeys, M., Koch, R., Vergauwen, M., & Van Gool, L. (1999). Hand-held acquisition of 3D models with a video camera. *Proceedings of the 2nd International Conference on 3D Digital Imaging and Modeling*, 14-23. https://doi.org/10.1109/IM.1999.805330

[10] Fischler, M. A. & Bolles, R. C. (1981). Random sample consensus: A paradigm for model fitting with applications to image analysis and automated cartography. *Communications of the ACM*, *24*(6), 381-395. https://doi.org/10.1145/358669.358692.

[11] Tomasi, C. & Kanade, T. (1992). Shape and motion from image streams under orthography: A factorization method. *International Journal of Computer Vision*, *9*(2), 137-154. https://doi.org/10.1007/BF00129684.

[12] Lhuillier, M. & Quan, L. (2005). A quasi-dense approach to surface reconstruction from uncalibrated images. *IEEE Transactions on Pattern Analysis and Machine Intelligence*, *27*(3), 418-433. https://doi.org/10.1109/TPAMI.2005.44

[13] Lowe, D. G. (1999). Object recognition from local scale-invariant features. *Proceedings of the International Conference on Computer Vision*, 1150-1157. https://doi.org/10.1109/ICCV.1999.790410

[14] Brown, M. & Lowe, D. G. (2007). Automatic panoramic image stitching using invariant features. *International Journal of Computer Vision*, *74*(1), 59-73. https://doi.org/10.1007/s11263-006-0002-3

[15] Mikolajczyk, K. & Schmid, C. (2005). A performance evaluation of local descriptors. *IEEE Transactions on Pattern Analysis and Machine Intelligence*, *27*(10), 1615-1630. https://doi.org/10.1109/TPAMI.2005.188.

[16] Bay, H., Ess, A., Tuytelaars, T., & Van Gool, L. (2008). Speeded-up robust features (SURF). *Computer Vision and Image Understanding*, *110*(3), 346-359. https://doi.org/10.1016/j.cviu.2007.09.014

[17] Rosten, E. & Drummond, T. (2006). Machine learning for high-speed corner detection. *Proceedings of the European Conference on Computer Vision*, 430-443. https://doi.org/10.1007/11744023_34

[18] Shi, J. & Tomasi, C. (1994). Good features to track. In *Proceedings of the IEEE Conference on Computer Vision and Pattern Recognition*, 593-600. https://doi.org/10.1109/CVPR.1994.323794

[19] Szeliski, R. (2010). *Computer vision: Algorithms and applications*. https://doi.org/10.1007/978-3-030-34372-9

[20] Amidžić, O., Riehle, H. J., & Elbert, T. (2006). Toward a psychophysiology of expertise: Focal magnetic gamma bursts as a signature of memory chunks and the aptitude of chess players. *Journal of Psychophysiology*, *20*(4), 253-258. https://doi.org/10.1027/0269-8803.20.4.253.

Contact information:

Mingbo LIU
Department of Obstetrics and Gynecology,
Chongqing Health Center for Women and Children,
Women and Children's Hospital of Chongqing Medical University,
Chongqing, China

Tieyuan SUN
Department of Obstetrics and Gynecology,
Chongqing Health Center for Women and Children,
Women and Children's Hospital of Chongqing Medical University,
Chongqing, China

Ye HAN
Department of Obstetrics and Gynecology,
Chongqing Health Center for Women and Children,
Women and Children's Hospital of Chongqing Medical University,
Chongqing, China

Jianshuang LIU
Department of Obstetrics and Gynecology,
Chongqing Health Center for Women and Children,
Women and Children's Hospital of Chongqing Medical University,
Chongqing, China

Xiaolong YOU
Department of Optical Measurement and Navigation,
PhySoft Research Group, Chongqing, China

Lubin LIU
(Corresponding author)
Department of Obstetrics and Gynecology,
Chongqing Health Center for Women and Children,
Women and Children's Hospital of Chongqing Medical University,
Chongqing, China
E-mail: liulubin1975@126.com